Available online at www.sciencedirect.com
SCIENCE DIRECT
Thermochimica Acta 414 (2004) 243–253
thermochimica acta
www.elsevier.com/locate/tca

Studies of structures of poly-ε-caprolactam/montmorillonite nanocomposite Part 1. Tests of compression moulded specimens

B. Jurkowski [a,*], Y.A. Olkhov [b]

[a] *Plastic and Rubber Processing Division, Institute of Material Technology, Poznan University of Technology, Piotrowo 3, 61-138 Poznan, Poland*
[b] *Institute of the Problems of Chemical Physics, Russian Academy of Sciences, 142 432 Chernogolovka, Moscow Region, Russia*

Received 24 September 2003; received in revised form 7 January 2004; accepted 7 January 2004

Abstract

A poly-ε-caprolactam (PA6) taken as a reference and its nanocomposite (PNC) containing 1.6 wt.% of montmorillonite were examined. The specimens as discs were prepared by compression moulding at 235 °C and 70 MPa. Using the novel version of TMA, in the PA6 and PNC specimens, within the temperature range from −100 to 250 °C, a semi-crystalline structure with anisotropy of distribution of the more ordered (crystalline?) portion was found in the surface layer up to 0.5 mm thick. The amorphous regions have differed in a state of order (different transition temperatures) and related compactness. The free volume fraction in amorphous regions determined in machine direction (normal to the surface) is increased when in transverse direction is reduced; simultaneously molecular weights of polymer chains between junctions were increased by incorporation of the nanofiller.

Keywords: TMA; PA6; Montmorillonite; Nanocomposite; Topological structure; Molecular structure; Pseudo-network

1. Introduction

Polymer nanocomposites (PNC) are materials with the substantially enhanced product performance [1–3]. By definition, PNC is a material that comprises a dispersion of nanometre-size particles in a polymer matrix. The nano-particles may be lamellar, fibrillar, shell-like, spherical, etc. However, the great majority of PNCs are based on clays. The most popular nano-clay is montmorillonite (MMT) made of three-layer sandwiches (tetrahedral/octahedral, etc.), each 0.96 nm thick, separated by a weakly bonded gallery filled with water molecules and mobile cations, such as Na^+. The clay has the cation exchange capacity CEC = 0.85–1.4 meq/g, aspect ratio p = 10–1000 and the specific surface area $S \cong 800\,m^2/g$. Since PNC performance depends on the aspect ratio (p: platelet diameter/thickness) of filler, the specific surface area and the particle–matrix interactions, the major goal for the technology of PNC manufacturing is to ascertain full *exfoliation* of clay in the polymer matrix. *Exfoliation* usually proceeds in two steps: *intercalation* that exchanges the mobile Na^+ for organic cations that ionically bond to the sandwich surface and expands the gallery, and the final *exfoliation* that disperses and randomizes the individual platelets in a matrix with the distance between them in excess of 8.8 nm [4]. Mentioned above intercalation is the ability of the polymer chains to enter the gallery spacings as exfoliation is achieved when the layer structure is delaminated and the platelets are uniformly dispersed in the polymer matrix.

At loading levels of 2–5 wt.%, PNC offers a similar performance to that of conventional composites with 30–50 wt.% of reinforcing filler. For example, PNC of PA6 containing 4.2 wt.% MMT shows the following improvements of the matrix performance at room temperature: tensile modulus by 73%, tensile strength by 41%, and heat distortion temperature by 87 °C [5]. In composites the high filler loading causes undesirable increase of density, decreases melt flow and increases brittleness. Furthermore, the composites are opaque with poor finish of a surface. These problems are

* Corresponding author. Tel.: +48-61-878-2771; fax: +48-61-878-2217.
E-mail addresses: boleslaw.jurkowski@put.poznan.pl, jurkowsk@sol.put.poznan.pl (B. Jurkowski).

0040-6031/$ – see front matter © 2004 Elsevier B.V. All rights reserved.
doi:10.1016/j.tca.2004.01.008

absent in PNCs if a predominately exfoliated structure is obtained. Cost differential between the neat matrix and its PNC is about 10–20%. PNCs main market is in the transport industries, with growing demand for packaging, machine manufacturing, building and construction, electrical and electronic, lawn and garden, power tools, etc. Advantages of nanocomposites range from enhancement of mechanical performance [5–8] to reduction of permeability and flammability [9–11], better optical properties, modification of magnetic, electric or light-transmitting performance, biocompatibility, thermochromic effects, better resistance to ageing and environmental degradation [7], etc.

Considering the growing importance of these materials to the global economy, it is necessary to investigate effective ways for the optimization of formulation and compounding technology of nanocomposite. To make them more efficient it is necessary to develop new methods for selecting the characteristics of composite structure to maximize their most desirable properties for specific applications. One of such methods could be the topological structure evaluation by the thermomechanical analysis (TMA).

The motivation for this work was to complement the study of structure and properties of poly-ε-caprolactam (PA6) nanocomposites as an extensively studied model system. Thus, two commercial materials, neat PA6 and based on it PNC are used. The latter material contains 2.0 wt.% of organoclay (MMT intercalated with ω-amino dodecanoic acid) or 1.6 wt.% (i.e. 0.64 vol.%) of MMT. Owing to the reactive exfoliation method and the polar nature of PA6, the clay is exfoliated and individual MMT platelets are uniformly dispersed in the polymer matrix. TEM shows that MMT frequently has the adjacent layer crystallographically welded together. In the PA6 matrix the platelet cross-section is seen not as a line but a branched structure. Thermodynamic interactions within the system and the molecular structure were recently characterized using the pressure–volume–temperature measurements and the analysis by means of the equation of state [12,13]. The work shows strong interaction between clay and PA6 that caused solidification of chains on the platelet surface well above the bulk melting point. One of the results of this behaviour is ca. 14–16% reduction of the free volume fraction of PA6 caused by the addition of 0.64 vol.% of exfoliated clay.

The rheological studies [14] inform that about 1/3 of MMT anions directly bonds to PA. The number of chains attached to a single clay platelet is ca. 47,000, thus, the structure is named a “hairy clay platelets (HCP)”. Since the platelets have high aspect ratio $p = 286$, HCP flow behaviour resembles that of the liquid crystal polymers (LCP). As LCP, the HCP also aggregate into assemblies that at low deformation rate respond similarly like a 3D network, at mid-flow rates the assemblies tumble and slowly disintegrate, then at high rates HCPs became oriented.

Incorporation of exfoliated MMT into PA6 enhances nucleation that accelerates crystallization and modifies the crystalline form from α to γ [15,16]. The elastic modulus, yield stress, and strain at break are sensitive to the filler content and orientation [16,17]. In consequence, one may expect that the TMA will be able to characterize the orientation, since orientation influences the topological structures in PA6/MMT nanocomposite.

2. The model

Low frequency test methods would have the highest resolution power when scanning a polymer for multiple transitions [18]. Because of this, the TMA method is sensitive to changes in the elastic modulus and it provides [19–21] numerous molecular and topological characteristics from the analysis of thermomechanical curves (TMC). The TMC could be approximated as lines with several breaks separating the apparently linear segments with varied slopes, what informs about existence of material regions having different thermal expansion properties. Based on this fact, it is possible to assume that these regions differ in degree of order or interaction energies. Such plots from early years of polymer science served as a qualitative evidence for multiple transitions in semi-crystalline polymers.

The new version of TMA has been used in studies of linear (having a physical pseudo-network called also a temporary network) and crosslinked polymers, co-polymers and composites, as well as, interpenetrating and semi-interpenetrating networks, and rubbers [22–39]. There is attempted to associate each TMC break with a characteristic change in the thermal expansion properties and related free volume fraction of particular amorphous regions in polymer structure.

The new approach is based on a simplified model network with physical and/or chemical junctions, which accounts for different thermal expansions in different zones (linear segments) of TMC. Thus, the TMC may be used to characterize quantitatively a polymer topological structure; it means regions having complex associated structures with higher-level organization than the molecular one. Architecture with two or three amorphous regions (e.g. in the volume between adjacent lamellae), probably interpenetrating [18] is found. These regions are not divided in space; they represent several types of interactions, which coexist in polymers. They differ in the transition temperatures up to 200 °C and related compactness [26–29]. Since the degree of order influences diffusivity of low-molecular substances [40], the two amorphous regions found in most tested composites cause a heterogeneous distribution of ingredients hence materials performance.

So far, nanocomposites have not been studied by means of TMA to evaluate their topological and molecular characteristics. This method may offer some additional information for the optimization of multi-phase, multi-component materials that progressively dominate the polymer industries [41–43].

Thermodynamics of arbitrarily chosen process requires that for the free energy to reach its minimum value, the entropy and enthalpy must change. Thus, during melting, the enthalpy and specific volume changes. Some of the commonly used methods for the determination of crystallinity (DSC and dilatometry) are based on measurements of these properties [44–46]. However, these results are volume-averaged, suffering from many experimental and structural errors.

Comparison of X-ray diffraction and DSC results shows that the TMA is useful to evaluate the degree of crystallinity in thin (up to 0.5 mm thick as calculated by using finite elements analysis) layer of the polymer specimen [47]. The contact surface area is ca. 0.17 mm^2. Because of this, the information about polymer properties is an average on this surface and depth.

Thus, to discuss results obtained by the TMA it is necessary to know the thermal and stress history of the specimen. We expect that information obtained at orthogonal directions may be used for determination of topological anisotropy of polymeric materials.

3. Experimental

3.1. Materials

The two commercial materials were supplied by the Ube Industries Ltd. However, we did not obtain the information on properties of the nano-clay used. The specimens as discs were prepared according to following procedures.

The first specimen was well dried PA6 (Nylon 1015B, $\bar{M}_n = 22$ kg/mol, heat deflection temperature HDT = 75 °C and flexural elastic modulus $E = 285$ MPa). It was compression moulded in a Carver laboratory press for 5 min at the temperature $T = 235$ °C and pressure $P = 70$ MPa. Then the press plates were cooled by cold water, pressure release and specimens removed from the mould. The solidification was fast as the crystallization temperature is about 200 °C and proceeds without a contact with ambient air contrary to that described in the second part of this article.

The second specimen was well dried PNC (Nylon 1015C2 containing 1.6 wt.% of exfoliated clay in PA6 matrix, having $\bar{M}_n = 22$ kg/mol). It was compression moulded as above. By comparison with neat PA6, the PNC has density higher by ca. 1%, HDT = 140 °C increased by 65 °C and E = 359 MPa increased by 26%.

3.2. Methodology

The TMA is based on measurements of the deformation of specimen under low load during the temperature increase, what gives the TMC. Analysis of the TMC leads to determination of transition temperatures, degree of crystallinity, and shares of regions differing by thermal expansion. Furthermore, the published procedure proved experimentally by using model networks [36,39] makes possible to calculate molecular weight (MW) and molecular weight distribution (MWD) of the chain segments between junctions in the pseudo-network in particular region.

The lower surface of the specimen contacts a base of the thermostatic chamber of UIP-70M apparatus made by the Central Design Bureau of the Russian Academy of Sciences, Moscow, and the upper is probed with a measuring probe, the surfaces should be parallel. The procedure is as follows: the specimen (ca. 1 mm thick plate 3–5 mm in diameter) is placed in the measuring cell of the thermostatic chamber. It is cooled down (without pressure) at a rate 4 °C/min from room temperature to ca. $T = -130$ °C, then kept at this temperature for 10–15 min to equalize a thermal field within a specimen. To ensure reversibility, the applied initial specimen deformation H (obeying Hooke's law) is smaller than 5% of a radius R of the probe's tip, it means below 0.05 mm. To obtain the TMC, the probe 2.0 mm in diameter with a hemispherical tip and with constant load of 0.1–0.5 g (minimum for the instrument) is lowered to contact with the surface of specimen. This minimum load is determined by the sensitivity of TMA measuring load cell.

The heating is carried out at the same rate as the cooling and lasts until the specimen either starts to flow (for linear polymers), or to degrade (for crosslinked polymers). During the heating, the varying deformation of specimen (usually $\Delta H \leq 0.1$ mm) is measured. Such deformation is a sum of the linear thermal expansion and the thermomechanical deformation resulted from penetration of the probe. The direction of the thermal expansion is opposite to the thermomechanical deformation.

Coefficients of linear thermal expansion below (α_1) and above (α_2) the glass transition temperature (T_g) have been determined at non-equilibrium conditions from the TMC as slopes of straight lines portions of the curve within the glassy and rubbery state, respectively. $\alpha = (\Delta H/H_0)/\Delta T$, where $\Delta H/H_0$ is a relative change of an initial height H_0 (specimen thickness) within the temperature interval, ΔT.

There are several methods of evaluation of voids volume, but they give results differing even three times or more [18]. One of them uses α values below and over the glass transition to evaluate the so-called "free volume fraction, V_f" of amorphous polymers at T_g, being related to their cooperative entropical changes, according to empirical [18,48] dependence:

$$V_f \approx 3(\alpha_2 - \alpha_1)T_g \approx \text{const.} \approx 0.113 \quad (1)$$

Here it is accepted that volumetric thermal expansion coefficient is equal to three linear one, material is isotropic and sizes of voids are similar in three directions. This dependence was elaborated for polymers in iso-free state (a not fulfilled condition) [18,49,50], or proposed by Privalko [50] its adjusted version as

$$V_f \approx 3\Delta\alpha T_g \left(1 - \frac{T_2}{T_g}\right) \quad (2)$$

where T_2 is the hypothetical temperature of the equilibrium second order transition and $\Delta\alpha = \alpha_2 - \alpha_1$.

Eq. (1) has been deeply discussed by Lipatov [49] and Privalko [50]. Lipatov termed it as *geometrically* free volume fraction (ca. 10–15% of specimen). However, the above value varies for particular polymer depending on its molecular weight, crosslinking degree and rigidity of chains [18,50], conditions of formation of its structure [51], and on evaluation method [18,49,50] what limits its usability. For rubbery materials $V_f \approx 0.113$, when for rigid-chain polymers $V_f > 0.113$ and for soft-chain crystallizable polymers $V_f < 0.113$. Simultaneously, physically free volume fraction, determined by relaxation times (ca. 3% of specimen volume) has been discussed [49]. Its variation is lower than that of geometrically free volume.

The free volume usually is evaluated [52,53] by using the following expressions:

$$3\Delta\alpha T_g = \left[\frac{\varepsilon_h}{RT_g}\right] \exp\left[-\frac{\varepsilon_h}{RT_g}\right] \tag{3}$$

$$\frac{\varepsilon_h}{RT_g} \approx -\ln V_f \tag{4}$$

where ε_h is the energy of hole formation. Volume of voids visible on a surface of material also could be evaluated from AFM images, but it is much larger than determined by above methods.

Interval $0.092 \leq 3\Delta\alpha T_g \leq 0.117$ correspond to $0.025 \leq V_f \leq 0.035$ [54], what make possible to find the empirical scaling factor, $(0.092 + 0.117)/(0.025 + 0.035) = 3.48$ of the experimental values of $3\Delta\alpha T_g$ from TMA (Table 1) and V_f from expressions (3) and (4). Considering this, we obtain a corrected version of the dependence (1) as

$$V_f \approx 0.86(\alpha_2 - \alpha_1)T_g \tag{5}$$

Distribution of voids within a polymer is not uniform that allows different motions [49]. Because of this, particular T_g could correspond to different statistical distribution functions of voids due to variations in a structure of polymer.

Based on data of Ferry [55] and two ways of statistical calculations on three sigma level (99% confidence limit), it has been found that the ratio of the thermal expansion coefficients below and above T_g at the same heating rate $\alpha_2/\alpha_1 \leq 5.12$ for unfilled polymers could be preliminary accepted as a criterion that this structure is amorphous [56]. The ratio $\alpha_2/\alpha_1 > 6.24$ is typical for crystalline and semi-crystalline materials.

The TMC may be recorded in machine (or normal to the surface of specimen) $MD^{\parallel}$ and transverse direction $TD^{\perp}$, respectively, to evaluate anisotropy of material structure. One measure of anisotropy is the ratio K_a of the amount of ordered portion in parallel ($\varphi^{\parallel}$) and perpendicular ($\varphi^{\perp}$) direction to that used during specimen manufacturing:

$$K_a = \frac{\varphi^{\parallel}}{\varphi^{\perp}} \tag{6}$$

The transitional zone of the TMC is caused by polydispersity of lengths of the chain segments between junctions of the polymer network or pseudo-network. Molecular weight of them is directly proportional to a value of ΔT according to the empirical relation [19]:

$$\log M_{min} = 2.3 + \frac{11\Delta T}{100 + \Delta T} \approx 10^4 \tag{7}$$

where M_{min} is the lowest molecular weight of polymer segments between junctions in the polymer network or pseudo-network, which start to flow in loaded specimen at temperature T_{min} [19,37,57–59]. M_{min} is directly proportional to $\Delta T_{min} = T_{min} - T_g$. For the highest molecular weight segments, this process begins at T_∞. It means M_{max} is directly proportional to $\Delta T_{max} = T_\infty - T_g$.

If the straight-line segment of TMC that describes the melting process of crystalline portion does not end by a deformation curve (low temperature crystalline portion), it is assumed that between junctions of this portion of polymer $\bar{M}_w = \bar{M}_n$. In polar and highly viscous polymers, $\bar{M}_n$ is evaluated only. The transitional zone of the TMC could begin immediately after T_g what is shown in Fig. 1(a) and (b) as the curve BC. It also could be combined from linear segment CD describing rubbery properties and the curve DO. In Fig. 1, point D is accepted as the end of straight-line segment.

The equilibrium high-elastic modulus, E_∞, correspond with a plateau of high-elasticity in amorphous region of a polymer. The crosslink density ν_e in a pseudo-network of amorphous regions could be calculated [60–62] from the expressions:

$$\nu_e = \frac{E_\infty}{3RT} \tag{8}$$

where R is the gas constant and T is the temperature or

$$\nu_e = \frac{\rho}{\bar{M}_n} \tag{9}$$

where ρ is polymer density and $\bar{M}_n$ is the number-average molecular weight.

Many characteristics from the TMA are correlated satisfactory ($r \geq 0.7$) with mechanical properties [63–65]. However, molecular weight evaluated by the TMA for particular topological region is different from the global value determined by methods when testing of dissolved material. It could be resulted from changes of intermolecular interactions due to a difference in testing temperature and penetration of solvent molecules between neighbouring segments of polymer chains. In addition, entanglements would act differently in molten polymer than in its low viscous solution.

3.3. Accuracy and reproducibility

The accuracy of the temperature measurements in thermostatic chamber of the instrument is $\pm 0.05\,^{\circ}C$, but within a specimen may vary due to differences in local heat trans-

Table 1
Molecular and topological structures of PA6 and its nanocomposite (PNC)

Analysed parameter[a] (95% confidence limit)	PA6		PNC	
	∥[b]	⊥[b]	∥	⊥
Low-temperature amorphous region				
T_g, °C (±3 –5)	−14	−13	−6	−14
$\alpha_1 \times 10^5$, deg^{-1} (±10%)	6.0	2.6	6.2	2.3
$\alpha_2 \times 10^5$, deg^{-1} (±10%)	24.0	15.5	26.6	9.7
V_f (±10%)	0.140	0.101	0.157	0.057
$\bar{M}'_w$, kg/mol (±10%)	9.7	33.9	4.5	12.3
K' (±10%)	1.41	1.64	1.44	1.72
E_∞, MPa (±10%)	1.92	0.63	3.0	1.72
$\nu_e \times 10^4$ (±10%)	1.60	0.53	3.40	1.54
φ' (±10%)	0.31	0.94	0.19	0.85
High-temperature amorphous region				
T_{htt}, °C (±3 –5)	–	–	–	166
V_f (±10%)	–	–	–	0.096
$\bar{M}''_w$, kg/mol (±10%)	–	–	–	158.5
K'' (±10%)	–	–	–	1.59
T_f, °C (±3 –5)	–	–	–	201
φ'' (±10%)	–	–	–	0.15
Low-melting crystalline portion				
T'_m, °C (±3 –5)	46	–	42	–
$\alpha_3 \times 10^5$, deg^{-1} (±10%)	47.1	–	59.5	–
$\bar{M}'''_w$, kg/mol (±10%)	45.5	–	4.5	–
K''' (±10%)	1.52	–	–	–
φ''' (±10%)	0.67	–	0.11	–
Intermediate-melting crystalline portion				
T''_m, °C (±3 –5)	–	–	119	–
$\alpha_3 \times 10^5$, deg^{-1} (±10%)	–	–	40.3	–
$\bar{M}'''_w$, kg/mol (±10%)	–	–	1780	–
φ'''' (±10%)	–	–	0.34	–
High-melting crystalline portion				
T'''_m, °C (±3 –5)	202	198	139	–
$\alpha_5 \times 10^5$, deg^{-1} (±10%)	47.1	39.5	48.1	–
$\bar{M}''''_w$, kg/mol (±10%)	3.0	2.5	2500	–
K'''' (±10%)	1.67	1.54	–	–
T_f, °C (±3 –5)	206	208	201	–
φ'''' (±10%)	0.02	0.06	0.36	–
Values averaged between regions[c]				
$\bar{M}_w$, kg/mol (±10%)	33.5	32.1	1500	41.2

[a] $K = \bar{M}_w/\bar{M}_n$, polydispersity index; $\bar{M}_w$, the weight-average molecular weight; $\bar{M}_n$ is the number-average molecular weight, T_f the temperature of the beginning of molecular flow, T_g the glass transition temperature, T_{htt} the high temperature transition, T_m the temperature of the beginning of melting process, V_f the free volume fraction calculated as equal to $3\Delta\alpha T_g$, $\Delta\alpha = \alpha_2 - \alpha_1$, α_1 the coefficient of linear thermal expansion in a glassy state, α_2 as α_1 but in a high-elastic state, low-temperature region, α_3 the coefficient of linear thermal expansion during melting of low-melting crystalline portion, α_4 as α_3 but for high-melting crystalline portion, φ—a weight share of the region.

[b] Orientation in machine direction (MD) or parallel to stress (∥) or normal to the surface of specimen and in transverse direction (TD) or perpendicular to stress (⊥).

[c] Averaging was performed using weight shares of the regions and respective $\bar{M}_w$ magnitudes.

fer. The accuracy of deformation is ±5 nm. Taking into account some non-uniformity of specimens and other variations, the characteristic temperatures are determined with accuracy ±3 to 5 °C. Consequently, the errors of E_∞, MW, and free volume fraction are less than or equal to ±10%.

The data were reproducible within the error limits of ±5 to 10%, but in some cases, it can be as large as ±20% due to heterogeneity of the materials and differences in their thermal and stress history.

4. Results and discussion

4.1. Topological and molecular structures of PA6 specimen tested in MD^{II}

The thermomechanical curve for neat PA6 shown in Fig. 1 has been recorded from −100 to 220 °C (beginning of flow). It has a typical shape for a semi-crystalline polymer. Thus, between temperature of the beginning of test equal −100 °C

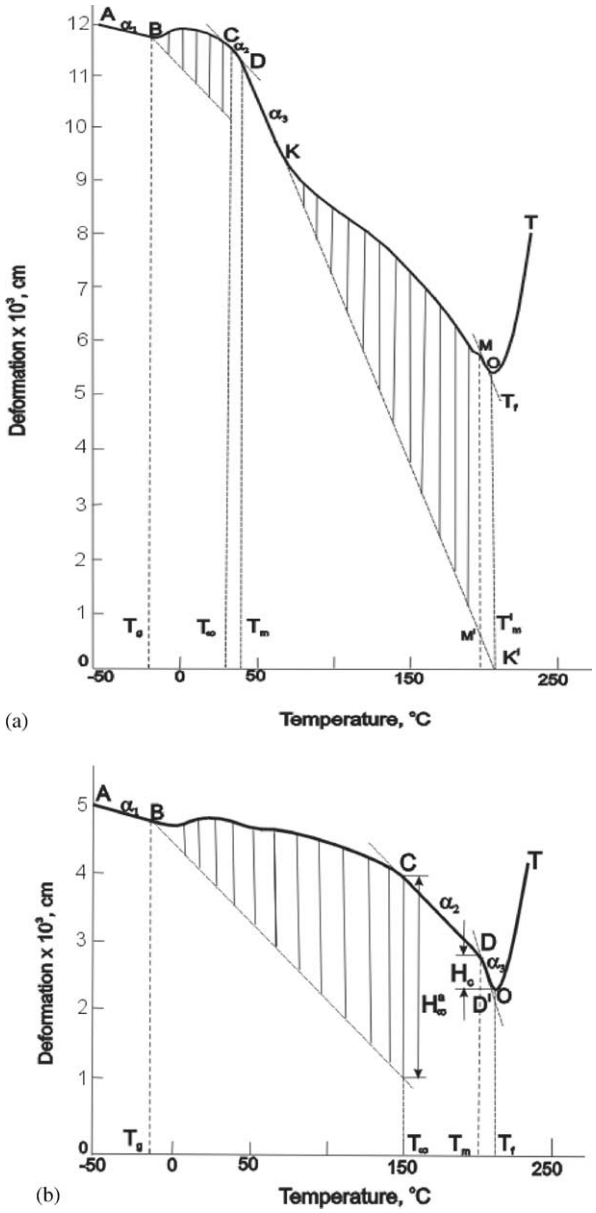

Fig. 1. The thermomechanical curve for compression moulded neat PA6 tested in (a) MD^{II} and (b) $TD^{\perp}$ test directions.

and $T_g \cong -14\,^{\circ}C$, PA6 is in a glassy state and, due to this, it expands linearly when heated at a constant rate (the straight line AB). The coefficient of linear thermal expansion in this zone, $\alpha_1 = 6.0 \times 10^{-5}\,deg^{-1}$.

At T_g (point B in Fig. 1), the segmental mobility in a pseudo-network starts to increase and a transitional zone begins (the curve BC of the TMC). This zone originates from the thermomechanical deformation under applied load and it characterizes a structure of the amorphous region. The observed changes are resulted from the thermal disintegration of physical junctions in the pseudo-network, which lowers the elastic modulus. The theory of the TMC analysis [33–35] and the physical networks [66] relates the transitional zone to MWD of the chain segments between junctions of the polymers' network in the amorphous part. Thus, it is possible to evaluate MWD and to calculate the number-average and the weight-average molecular weights of chain segments between junctions in the amorphous region [36,39].

The transitional zone of the TMC ends at temperature corresponding to point C and the polymer begins for the second time to expand linearly because of increasing the free volume [34]. This zone corresponds to the elastic plateau, i.e. it is a zone of relatively stable pseudo-network of amorphous topological region of PA6 (the zone CD). It is assumed by TMA methodology that TMC between points A and D characterizes the first amorphous region in glassy and rubbery states. In many cases, two amorphous regions with different transition temperatures could be observed. Usually zone CD is quite long to determine accurately a slope of the straight-line segment of the curve (Fig. 1(b)). If it is short, as in Fig. 1(a), it has been assumed that it describes a small amount of an amorphous portion with determined roughly a ratio of α_2/α_1 usually on the level between 2.5 and 3. However, such interpretation needs some additional information about existence of amorphous structure from independent measurements. The expansion rate of a polymer in this zone is constant and equal to the coefficient of linear thermal expansion within the rubbery region, $\alpha_2 = 2.4 \times 10^{-4}\,deg^{-1}$. Based on statistical studies [56] it has been expected that the physical junctions in a pseudo-network of amorphous topological region could be PA6 crystallites.

The principal expansion zone of PA6 starts at the temperature corresponding to point D on the TMC. This rapid expansion, with the straight line DK dependence giving the thermal expansion coefficient $\alpha_3 = 4.7 \times 10^{-4}\,deg^{-1}$, and ratio $\alpha_3/\alpha_1 > 6.24$, corresponds to melting of a crystalline portion [40,55,56]. PA6 specimen after termination of compression moulding has been cooled in the mould together with heating plates. Due to high heat capacity of metallic plates and mould, a substantial lowering of specimen temperature begins after some period from the beginning of flow of the cooling water. Because of this, for crystallizable polymers during this period, it is observed some crystallization on the surface of specimen before solidification. Inner part of it is preserved at crystallization temperature during longer period, what results in a gradient of crystallization degree across the specimen. Given above interpretation of the TMC agrees with common knowledge that PA6 is a semi-crystalline polymer. If some assumes that a segment CK describes properties of one topological region of the polymer instead of two regions discussed above it will be equal with acceptance of its crystalline structure, what is contradictory with well-known literature data. From this, it is concluded that interpretation of the TMC in the last two paragraphs is reasonable.

At the temperature marked by point K in Fig. 1(a), the melting expansion (following the straight line DK) starts

to be complicated by a thermomechanical deformation, H_i, caused by essential penetration of the measuring probe into the melting specimen. It may be shown that, similarly as for amorphous polymers [57], within the transitional zone KM successive fractions of different molecular weight are being activated (melted), thus, under assumption of apparent equilibrium, one may compute the MWD of the chain segments between the network junctions. However, the results depend also on the compressive stress/elastic modulus ratio, P/E [39]. Thus, the TMC within the KM interval depends not only on the MWD, but also on the P/E ratio. The last one may also influence the calculated MWD.

The increase in temperature from T_g to T_8 in Fig. 1(a) causes all of these deformation jumps at successive temperatures, T_i, that reduces the elastic modulus. The process is attributed to a sequential transition of different MW $= M_i$ of polymer segments between junctions (starting from the lowest to the highest MW) into the molten state. When the temperature reaches T_∞, the equilibrium deformation H_∞ is obtained before the test ends. As it was pointed out above, M_i is directly proportional to $\Delta T_i = T_i - T_m$ [19,37,57–59]. In a pseudo-network of PA6 the amorphous regions are linked by the thermally stable crystalline regions, which begins to melt at $T'_m = 202\,^\circ$C (point M).

The short straight-line segment MM′ of thermal expansion at melting of high-melting crystalline portion is visible as a zone of plateau of high-elastic deformation of this portion. It ends at temperature T_f corresponding with point O (minimum at the curve) at which elastic modulus of a polymer approaches zero-level and the polymer starts to flow (the curve segment OT). At T_f, the smallest chains begin to flow. However, at this temperature a polydispersive polymer would not flow under the standard processing conditions. Proper processing requires reaching a higher temperature ensuring a technological flow at given shear rate, at which the highest molecular weight fractions start to flow. Because of this, for a given polymer the wider the MWD the higher is the processing temperature. Analogous description of TMC of other polymers or polymeric composites could be made [28].

The calculated MWD of chain segments between junctions in amorphous and crystalline regions of PA6 are shown in Fig. 2. Both MWDs are bimodal enriched by smaller fraction of a high-molecular weight component. The molecular and topological characteristics of PA6 are listed in Table 1. There are four, three or two sets of data for MW between junctions in the pseudo-network of amorphous and crystalline regions depending on how it is tested. Their topological structure is determined by conditions of synthesis (chemical structure of polymer chains) and specimens manufacturing (different variation in stress and thermal fields). They are very different what is difficult to be explained without further experiments.

Data collected in Table 1 describe some molecular properties of particular amorphous and crystalline regions of

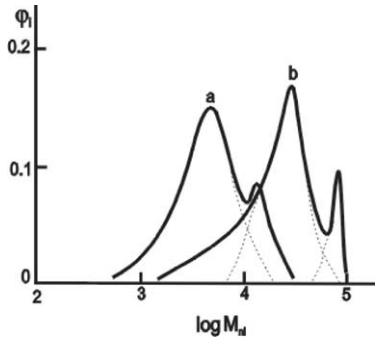

Fig. 2. Molecular weight distributions of the chain segments between junctions in a pseudo-network of amorphous (a) and crystalline (b) topological regions for compression moulded neat PA6 tested in MD^{II}.

solid PA6, but they are hardly to be compared with data from other methods, when usually dissolved polymer is tested and is accepted as a single-phase material. Dissolving essentially changes interactions between neighbouring chain segments, what suggests that characteristics from TMA should be different from such characteristic obtained in a liquid phase. However, to make some comparisons we also have averaged the MW between junctions of PA6 for all topological regions observed by the TMA. For this purpose it has been accepted that $\bar{M}_n = \bar{M}_w/K = 13$ kg/mol (Table 1). As expected, this value is lower than $\bar{M}_n = 22$ kg/mol determined by Ube Ind. for the bulk polymer, by means of a size exclusion chromatography (SEC) as the junction involves entanglements hence the average should be $\ll M_n$. The polydispersity indexes of PA6 for compared testing methods are similar, viz. $K = 2.6$ and 2.3, respectively, what is reasonable taking into account some differences in testing conditions and some error of MW evaluation.

The usually cited the glass transition temperature of PA6, $T_g = 50$–$75\,^\circ$C, as determined by, e.g. DSC, represents an average for all structures within the tested specimen. However, TMA detects several relaxation processes, which indicate that the onset of the thermal motion is associated with the transitions characterizing several topological regions and extending from -14 to $160\,^\circ$C (Table 1). This suggests an existence of a variety of structures differing in interaction energies. Similar conclusions might be made also for the melting temperatures, T_m.

4.2. Effect of test direction

The TMC for PA6 tested in $TD^{\perp}$ (Fig. 1(b)) has characteristics different from these in MD^{II} (Fig. 1(a)). However, in both cases the polymer structure is semi-crystalline what is evidenced by a ratio of thermal expansion coefficients in particular linear zones of the TMC. It is known that technological flow of molten polymer and compression of it at $P = 70$ MPa in the mould make some plane orientation of PA6 chains, mostly horizontal and radial out of the specimen centre. Because of this, an anisotropy of topological struc-

ture is expected, what was observed also by TMA testing of butyl rubber, Teflon, and many others (our unpublished data). This also agrees with known observations a structure of skin layer of rubber goods and tires, which are produced by compression moulding.

In Fig. 1(a) there is one amorphous region and two crystalline ones that substantially differ in T_m (Table 1), whereas in Fig. 1(b) there is one amorphous and one crystalline region. Note that the final test temperature, T_f, is almost the same in both tests. The numerical analysis of data shows a substantial difference in crystallinity depending on the test direction—the structure measured in MD^{II} gives the total crystallinity as $\sum \varphi^{\parallel} = 0.69$, whereas that in $TD^{\perp}$ is $\varphi^{\perp} = 0.06$. Determined by DSC total crystallinity of PA6 was about 50%. The difference could be explained by a fact that DSC is sensitive to crystalline phase independently on a size of crystalline formations. Thermal effects (area under peak) depend on a share of crystalline portion in the specimen. From this could be formulated hypothesis that the difference in crystallinity degree observed by DSC and TMA may be resulted from TMA sensitivity to aggregated crystalline formations, but not to micro- and nano-size such formations [67] and the thickness of polymer layer tested—in TMA up to 0.5 mm [47].

Furthermore, the anisotropy is also reflected in redistribution of the chains (giving different MW and MWD for the chain segments between junctions), as well as, the packing density. Macroscopically, these molecular-level differences result in specimen rigidity in two orthogonal directions. Thus, PA6 tested in MD^{II} is crystalline and in $TD^{\perp}$ is almost amorphous, and its low-temperature amorphous region is characterized by equilibrium elastic modulus of $E_\infty = 1.92$ and 0.63 MPa, respectively.

These values are significantly different from that quoted by the polymer manufacturer as the flexural bulk modulus, viz. $E = 285$ MPa (the tensile modulus for this PA6 is 1.1 GPa) when crystalline region (ca. 70 wt.%) presumably acts as reinforcing filler and networking agent what substantially influences macroscopic properties. How to explain such a difference in the elastic modulus? The reasons for it may be different testing conditions. First is a shape factor (SF) of a specimen equal to a ratio of its loaded surface to its free of load outer surface. For TMA tests SF $\approx 0.17\,mm^2/5–10\,mm^2 = 0.01–0.02$. For standard compression test using cylindrical specimen 30 mm in high and 12 mm in diameter it is quite different, namely SF $\approx 113/113 = 1$. Magnitude of SF strongly influences a side expansion of the specimen during compression due to changes in compressive stress distribution what influences a spatial distribution of strain and friction between a loaded surface of the specimen and loading plates or probe of the testing device. It has been found when testing rubber that for the higher SF elastic modulus at compression is essentially higher. A change from SF = 0.25 until 1.5 results in 2.5-fold increase in modulus at 10% compression, four-fold at 15%, and six-fold at 30%. The difference depends also on other

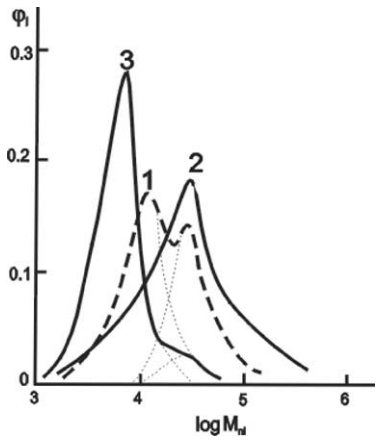

Fig. 3. Molecular weight distributions of the chain segments between junctions in a pseudo-network of amorphous topological regions in two different specimens of PA6 (curves 1 and 2) and PNC (curve 3) tested in $TD^{\perp}$.

factors like compression rate (for SF = 1 an increase in compression rate from 1.8 m/min till 5.6 m/min results in 45% increase of elastic modulus) and deformation [68]. During test at flexing, the distribution of stress is more determined, but also different from compression during TMA test. Second is testing temperature, which in a case of the TMA test for low-temperature region of PA6 it is equal $T_\infty = 80$ or 150 °C when for standard compression or flexing is room temperature. Third is time of measurements of deformation and speed of loading—for TMA it is static and equilibrium, for standard compression and flexural test speed of deformation is usually 5 mm/s. Fourth is accuracy of E_∞ evaluation. Data in Table 1 were evaluated basing on assumption that the Poisson ratio of neat PA6 and its nanocomposite is equal to 0.5. Such magnitude is acceptable for amorphous region, but not for crystalline when 0.3–0.35 is more proper. However, it is difficult to calculate an average Poisson ratio for semi-crystalline material, because the values could not be additive (influence of transitional layers). The fifth is the thickness of a material layer tested and related structure distribution. In TMA, it is up to 0.5 mm thick with different crystallinity degree than that that in the bulk. In macroscopically size specimens tested at compression or flexural mode it is different. All these reasons taken together (correction factor $E_{compr}/E_\infty \approx 3 \times 2 \times 2^6 \times 1.5 = 450$) make comparable E_∞ and E_{compr} values.

In Fig. 3 (the curves 1 and 2), MWD of the chain segments between junctions of the pseudo-network of amorphous topological regions in PA6 tested in $TD^{\perp}$ are presented. They could be bimodal or monomodal (however, a difference in modality could be resulted from scatter of evaluated MW), but show higher concentration of high-molecular weight fraction than that in $MD^{\parallel}$ (see Fig. 2, curve a). This evidences anisotropies in the tested specimens, supported also by the three-fold difference in the equilibrium elastic modulus (E_∞ in Table 1) for low-temperature amorphous region of PA6 at temperatures 80 and 150 °C.

4.3. Effect of MMT introduction

The PA6 nanocomposite, called PNC, contains 1.6 wt.% of MMT. The TMC for this material (Fig. 4) is similar to that of neat PA6 (Fig. 1(a)) tested in MD^{II}. Its topological structure contains amorphous pseudo-networked region with $T_g = -6\,^{\circ}C$ and three crystalline regions differing in temperatures of the beginning of melting: $T'_m = 42\,^{\circ}C$, $T''_m = 119\,^{\circ}C$ and $T'''_m = 139\,^{\circ}C$, as well as, in values of the respective thermal expansion coefficients: $\alpha_3 = 5.95\times10^{-4}\,deg^{-1}$, $\alpha_4 = 4.03\times10^{-4}\,deg^{-1}$, and $\alpha_5 = 4.81\times10^{-4}\,deg^{-1}$. The criterion for declaring preliminarily all three regions as crystalline is based on the ratio of thermal expansion coefficients during melting (relative slopes of the straight lines DD′, D′D″, and D″D‴) to α_1 in the glassy region (see line AB). The computed characteristics of topological structure are listed in Table 1. Characteristics of segments of chains between junctions of a pseudo-network in intermediate and high-melting crystalline portions of PNC are two orders of magnitude larger than molecular weight of neat PA6. However, the chain segments with molecular weight not higher than 20 kg/mol could create a low-temperature region in neat both PA6 and PNC. As it was mentioned above, incorporation of clay changes the crystalline forms of PA6 from more thermodynamically stable α- to γ-form [15,16]. The latter is created very rapidly due to nucleating ability of MMT and then slowly may transform back to α-form.

TMA is unable to evaluate a size of crystalline cell as it is during X-ray diffraction tests. However, analysing melting temperatures of different crystalline portions it is possible to make very preliminary conclusions about their amount. In the case studied, low-melting crystalline portion (67 wt.%) in PA6 transforms in PNC into another low-melting portion (only 11 wt.%), but with higher melting rate, it means with lower thermal stability. Simultaneously, introduction of MMT increases number of crystalline portions observed by TMA from two in PA6 to three in nanocomposite.

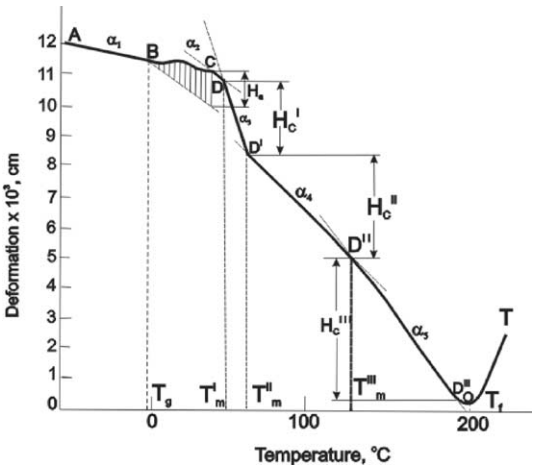

Fig. 4. The thermomechanical curve for compression moulded PNC tested in MD^{II}.

However, in PNC a total concentration of three crystalline portions $\sum 11\,wt.\% + 34\,wt.\% + 36\,wt.\% = 81\,wt.\%$ is higher than it was in PA6 using the same method of evaluation $\sum 67\,wt.\% + 2\,wt.\% = 69\,wt.\%$. From other methods [15,16], PNC crystallinity is also higher (60 wt.%) than that for PA6 (ca. 50 wt.%).

As shown in Table 1, the MW in the two crystalline portions detected by the TMA in nanocomposite is nearly three orders of magnitude higher than in neat PA6. This is a gratifying result as it is known [14] that in the PNC about 1/3 of chains is bonded to the MMT exfoliated platelets. Considering that the average diameter of clay platelet is nearly 300 nm, the number of end-tethered chains per MMT platelet is about 140,000, thus, the number-average MW of the "hairy clay platelet" is 1–3 Gg/mol. Furthermore, the crystalline surface of MMT strongly affects the segmental mobility. Within the PNC, the first 6 nm of PA6 (in the normal direction to the clay surface) is solidified. The chain mobility increases with distance from the clay platelet, but it takes 100–120 nm before bulk mobility would be achieved. At the clay loading in the tested specimens, the average distance between platelets is ca. 140 nm, thus, only a small fraction of PA6 enjoys the full thermal mobility [12,14]. This increases substantially the molecular weight of the physically networked polymer. Simultaneously, the total crystallinity degree of such a system determined by TMA tend to increase from $0.67 + 0.02 + 0.06 = 0.75$ for PA6 to $0.11 + 0.34 + 0.36 = 0.81$ for PNC (Table 1) what agrees with DSC measurements and is analogous to a case of rubber compounds. This fact is especially pronounced for crystalline high-melting portion, a weight share of which increases from 0.02 to 0.36. A new intermediate topological form with molecular weight that exceeds one million is evident in nanocomposites.

The TMC of compression moulded PNC tested in $TD^{\perp}$ (figure not given here) is different from that in MD^{II} (see Fig. 4). It shows a typical behaviour for an amorphous material with two regions differing in a degree of order and related transition temperatures. Topological structure of amorphous portion in PNC does not change with the direction of testing, MD^{II} or $TD^{\perp}$, but reductions of the free volume fraction V_f of amorphous portion and substantial increase in its share Φ is observed when testing in $TD^{\perp}$. The V_f in the amorphous portion of PNC has a value typical for crystallizable polymers, but different from that for neat PA6 (Table 1, low-temperature amorphous region tested in MD^{II} and $TD^{\perp}$ directions) what could be explained by some influence of MMT on non-perfect formation of a polymer structure.

Comparing the two TMCs it is evident that within the PNC specimen the crystalline portion is quite anisotropic, more so than what has been observed for PA6 specimen. This is also evident from data in Table 1. This agrees with a fact that MMT is known to enhance the rate of crystallization of PA6, to change the crystal type from α- to γ-form and to increase the degree of crystallinity [14,16,69].

The weight-average molecular weight $\bar{M}_w$ between junctions in topological regions tested in $TD^{\perp}$ is similar to that of neat PA6, but in MD^{II} it is much higher, what evidences (i) a substantial change in molecular weight between junctions of pseudo-network in PNC and (ii) partial transition into amorphous the less thermally stable crystalline structures during TMA test in $TD^{\perp}$. This also suggests that introduction of MMT and compression moulding applied makes some non-uniformity of junction's distribution in a pseudo-network of PNC—70% of it is included in a crystalline portion, but low dense networked. This could be one of the reasons for creation of the observed more elastic crystalline portion.

It is interesting to compare the MWD of the chain segments between junctions in a pseudo-network of amorphous regions of PA6 and PNC in MD^{II}—see curve (a) in Fig. 2 and curve (3) in Fig. 3, respectively. Both specimens have bimodal MWD, but in PNC, the high MW peak is much more pronounced, what should improve ultimate properties of materials [70]. This would indicate that high MW chain segments are more frequently found in PNC than in neat matrix, but at the same time the absolute magnitude of MW of the segments in PNC is smaller that that in PA6. The difference between the MWD of chain segments may indicate different types of networking junctions (chemical bonds gathered or not, or physical interactions) in these two specimens. This, by itself, is to be expected as the presence of MMT has large influence on the crystallinity, crystalline form of PA6 and the overall structure of the specimen [71].

5. Conclusions

1. Topological and molecular structures of PA6 and its nanocomposite evaluated by the novel version of TMA method respond differently, depending on the probing direction—in the direction of compression moulding (MD^{II} or parallel) and perpendicular to it ($TD^{\perp}$). The results provide evidence of anisotropy in spatial distribution of super molecular structures within the specimen. This explains why measuring in $TD^{\perp}$ in some cases did not detect crystalline portions, which are evident in MD^{II}. However, measuring in $TD^{\perp}$ most of information is collected from the layer up to 0.5 mm thick of the specimen when in MD^{II} it could be performed in deeper zone.
2. TMA tests on PA6 specimen performed in MD^{II} revealed its semi-crystalline topological structure with two crystalline portions. Its high-melting crystalline portion and amorphous region have isotropic spatial distribution, when crystalline low-melting portions are oriented in the plane perpendicular to the measuring probe, what gives some anisotropy in mechanical properties, i.e. E_{∞} at T'_m.
3. In PA6 nanocomposite containing 1.6 wt.% of exfoliated MMT unidirectional compression in moulding results in anisotropic topological structure containing one amorphous region and three more ordered (crystalline?) portions distributed non-uniformly in space and differing in morphology and related compactness. An anisotropic packing density of amorphous region has been shown as differences in the free volume fraction determined in two test directions. Differ also T_g magnitudes and E_{∞} at T_{∞} in the low-temperature amorphous region.
4. The free volume fraction of PA6 in the amorphous topological regions has been increased upon MMT addition. This disagrees with previous findings based on the analysis of PVT data [12]. Further detailed study of this phenomenon could explain why such composites have improved moisture resistance [69].
5. The nano-clay exfoliated and well dispersed within the matrix increases the apparent molecular weight of the chain segments between junctions. Such MW reaches a magnitude of some millions, what partly explains the reason for substantial improvement in mechanical properties observed by many researchers. This suggests also that nano-particles of MMT act as junctions of polymer pseudo-network.
6. Some orientation was observed for compression–moulded specimens of neat PA6. However, the degree of chain orientation does not reach such a level as it is for crystalline portion.

Acknowledgements

L.A. Utracki from NRCC/IMI in Canada supplied the specimens used in this work. We are very obliged for his fruitful discussion. The authors thank the Polish State Committee of Scientific Research (Grants 4 TO8E 067 25 and 4 T0 8E 067 25) for financial support.

References

[1] M. Alexandre, Ph.R. Dubois, Mater. Sci. Eng. 28 (1-2): 1-63, 2000.
[2] T.J. Pinnavaia, G.W. Beall (Eds.), Polymer–Clay Nanocomposites, Wiley, New York, 2001.
[3] L.A. Utracki, M.R. Kamal, Arabian J. Sci. Eng. 25 (2002).
[4] T. Lan, G.W. Beall, S. Tsipursky, US Patent, 6,057,396 (5 February 2000) to Amcol Intl. Corp.
[5] A. Usuki, in: Proceedings of the Polymer Nanocomposites 2001, NRCC/IMI, Boucherville, Que., Canada, 17 September 2001.
[6] K. Yasue, S. Katahira, M. Yoshikawa, K. Fujumoto, in: T.J. Pinnavaia, G.W. Beall (Eds.), Polymer–Clay Nanocomposite, Wiley, New York, 2001, p. 111.
[7] J.S. Shelley, P.T. Mather, K.L. DeVries, Polymer 42 (2001) 5849.
[8] J.M. Gloaguen, J.M. Lefebre, Polymer 42 (2001) 5841.
[9] J.W. Gilman, T. Kashiwagi, J.D. Lichtenhan, in: Proceedings of the 42nd International SAMPE Symposium, Anaheim Beach, 4–8 May 1997.
[10] H. Qin, Q. Su, S. Zhang, B. Shoo, M. Yang, Polymer 44 (2003) 7533.
[11] T.X. Liu, Z.H. Liu, K.X. Ma, L. Sheu, K.Y. Zeng, C.B. He, Comp. Sci. Technol. 63 (2003) 331.
[12] R. Simha, L.A. Utracki, A. Garcia-Rejon, Compos. Interfaces 8 (5) (2001) 345.

[13] L.A. Utracki, R. Simha, A. Garcia-Rejon, Macromolecules 36 (6) (2003) 2114.
[14] L.A. Utracki, J. Lyngaae-Jørgensen, Rheol. Acta 41 (2002) 394.
[15] X. Liu, Q. Wu, Eur. Polym. J. 38 (2002) 1383.
[16] M.N. Bureau, J. Denault, K.C. Cole, G.D. Enright, Polym. Eng. Sci. 42 (2002) 1897.
[17] K. Masenelli-Varlot, E. Reynaud, G. Vigier, J. Varlet, J. Polym. Sci. B: Polym. Phys. 40 (3) (2002) 272.
[18] R.F. Boyer, Rubber Chem. Technol. 36 (1963) 1303.
[19] Y.A. Olkhov, V.I. Irzhak, C.M. Baturin, RU Patent 1763952 (21 June 1993).
[20] Y.A. Olkhov, V.I. Irzhak, C.M. Baturin, RU Patent 2023255 (15 November 1994).
[21] Y.A. Olkhov, G.M. Bakova, A.S. Aleykinova, S.M. Baturin, RU Patent 1784861 (29 June 1993).
[22] Y.A. Olkhov, T.N. Smirnova, N.F. Kotova, L.I. Iskanov, V.K. Milinchuk, High Energy Chem. (RU) 223 (3) (1993) 13.
[23] Y.A. Olkhov, P.P. Kushch, in: Proceedings of the Second International Conference on Composites, Moscow, 1994, p. 238.
[24] Y.A. Olkhov, S.M. Baturin, Tech. Mashinenbuilding (RU) 4 (1995) 20.
[25] B. Jurkowski, Y.A. Olkhov, J. Appl. Polym. Sci. 65 (1997) 1807.
[26] B. Jurkowska, Y.A. Olkhov, B. Jurkowski, O.M. Olkhova, J. Appl. Polym. Sci. 71 (5) (1999) 729.
[27] B. Jurkowska, Y.A. Olkhov, B. Jurkowski, J. Appl. Polym. Sci. 68 (1998) 2159.
[28] Y.A. Olkhov, B. Jurkowski, J. Appl. Polym. Sci. 65 (1997) 499.
[29] B. Jurkowski, S.S. Pesetskii, Y.A. Olkhov, Y.M. Krivoguz, K. Kelar, J. Appl. Polym. Sci. 71 (1999) 1771.
[30] Y.A. Olkhov, D.G. Belov, G.P. Belov, Therm. Anal. 46 (1995) 237.
[31] N.G. Bazarnova, I.B. Katrakov, V.S. Kerneckii, Y.A. Olkhov, Plasticheskije Massy (RU) 8 (1998) 35.
[32] B. Jurkowska, Y.A. Olkhov, B. Jurkowski, O.M. Olkhova, J. Appl. Polym. Sci. 74 (14) (1999) 3305.
[33] T.F. Irzhak, S.E. Variukhin, Y.A. Olkhov, S.M. Baturin, V.I. Irzhak, Vysokomol Soed (RU) A39 (4) (1997) 671.
[34] Y.A. Olkhov, V.I. Irzhak, Polym. Sci. (RU) 40B (10) (1998) 1706.
[35] Y.A. Olkhov, S.M. Baturin, V.I. Irzhak, Polym. Sci. (RU) A38 (5) (1996) 849.
[36] B. Jurkowska, Y.A. Olkhov, B. Jurkowski, J. Appl. Polym. Sci. 74 (3) (1999) 490.
[37] B. Jurkowski, Y.A. Olkhov, B. Jurkowska, H. Menge, Polym. Test. 21 (5) (2002) 597.
[38] B. Jurkowski, Y.A. Olkhov, K. Kelar, O.M. Olkhova, Eur. Polym. J. 38 (6) (2002) 1229.
[39] Y.A. Olkhov, B. Jurkowski, B. Jurkowska, O.M. Olkhova, Eur. Polym. J., submitted for publication.
[40] L. Mandelkern, Crystallization of Polymers, Khimia Publishers, Moscow, 1966 (in Russian).
[41] L.A. Utracki, Two-Phase Polymer Systems, Hanser Publishers, Munich, 1991.
[42] L.A. Utracki, Polymer Alloys and Blends: Thermodynamics and Rheology, Hanser Publishers, Munich, 1990.
[43] I. Manas-Zloczower, Z. Tadmor (Eds.), Mixing and Compounding of Polymers, Hanser Publishers, Munich, 1994.
[44] M.I. Tetelbaum, Thermomechanical Analysis of Polymers, Nauka, Moscow, 1975 (in Russian).
[45] B. Wunderlich, Thermal Analysis, Academic Press, New York, 1990.
[46] T. Hatakeyama, F.X. Quin, Thermal Analysis, Chichester, Wiley, UK, 1994.
[47] J. Zielnica, P. Wasilewicz, B. Jurkowski, B. Jurkowska, Thermochim. Acta, submitted for publication.
[48] R. Simha, R.F. Boyer, J. Chem. Phys. 37 (5) (1962) 1003.
[49] Y.S. Lipatov, Uspiekhi Khimii (RU) 47 (2) (1978) 332.
[50] V.P. Privalko, Molecular Structure and Properties of Polymers, Khimia, Leningrad, 1986 (in Russian).
[51] Y.S. Lipatov, V. Posovizky, V. Babich, Eur. Polym. J. 13 (1977) 651.
[52] N. Hirai, H. Eiring, J. Appl. Phys. 29 (1958) 810.
[53] J. Moacanin, R. Simha, J. Chem. Phys. 45 (1966) 964.
[54] R.F. Boyer, R. Simha, Polym. Lett. 11 (1973) 33.
[55] J.D. Ferry, Viscoelastic Properties of Polymers, 3rd ed., Wiley, New York, 1980.
[56] B. Jurkowski, B. Jurkowska, K. Andrzejczak, Polym. Test. 21 (2) (2002) 135.
[57] S.S. Pesetskii, B. Jurkowski, Y.A. Olkhov, O.M. Olkhova, I.P. Strozhuk, U.M. Mozheiko, Eur. Polym. J. 37 (2001) 2187.
[58] R.G. Beaman, J. Appl. Polym. Sci. 9 (1952) 470.
[59] R.F. Boyer, J. Appl. Phys. 25 (1954) 825.
[60] W. Kuhn, Koll Z. 68 (1) (1934) 2.
[61] F.T. Wall, J. Chem. Phys. 10 (2) (1942) 132.
[62] L. Treloar, in: E.V. Kuvshinskii (Ed.), Physics of Rubber Elasticity, Moscow, Izdatinlit, 1953, p. 240 (in Russian, translation from English).
[63] B. Jurkowska, B. Jurkowski, J. Appl. Polym. Sci. 90 (9) (2003) 2583.
[64] B. Jurkowski, B. Jurkowska, in: Proceedings of the First Russian Rubber Conference, Moscow, 26–28 February 2002.
[65] B. Jurkowski, B. Jurkowska, in: Proceedings of the International Rubber Conference, Prague, 1–4 July 2002 (on CD) and Elastomery (Pl), vol. 6, No. 4/5, 2002, p. 3.
[66] V.I. Irzhak, G.B. Korolev, M.E. Soloviev, Uspiekhi Khimii (RU) 66 (1997) 179.
[67] V.A. Shershnev, I.K. Shundrina, V.D. Yulovskaya, Y.B. Evreinov, Kauchuk i Rezina (RU) 1 (1997) 16.
[68] J. Manuszak, Report for Polish State Committee of Scientific Research, 2002 (Grant No. 7 T07 B 043 15).
[69] M.R. Kamal, N.K. Borse, A. Garcia-Rejon, Polym. Eng. Sci. 42 (2002) 1883.
[70] J.E. Mark, J. Phys. Chem. B 107 (4) (2003) 903.
[71] L.V. Adamova, T.Y. Korniakova, A.A. Tager, I.S. Tiukova, V.A. Shershnev, I.K. Shundrina, V.D. Yulovskaja, Vysokomol Soed. (RU) 38A (8) (1996) 1362.